Neutral and ion chemistry in low pressure DC plasmas of H_2/N_2 mixtures: Routes for the efficient production of NH_3 and NH_4^+.

Esther Carrasco, Miguel Jiménez-Redondo, Isabel Tanarro and Víctor J. Herrero

Instituto de Estructura de la Materia, IEM-CSIC, Serrano, 123, 28006 Madrid (Spain)

E-mail: ecarrasco@iem.cfmac.csic.es

Abstract

The chemistry in low pressure (0.8-8 Pa) plasmas of H_2 + 10% N_2 mixtures has been experimentally investigated in a hollow cathode DC reactor using electrical probes for the estimation of electron temperatures and densities, and mass spectrometry to determine the concentration of ions and stable neutral species. The analysis of the measurements by means of a kinetic model has allowed the identification of the main physicochemical mechanisms responsible for the observed distributions of neutrals and ions and for their evolution with discharge pressure. The chemistry of neutral species is dominated by the formation of appreciable amounts of NH_3 at the metallic walls of the reactor through the successive hydrogenation of atomic nitrogen and nitrogen containing radicals. Both Eley-Rideal and Langmuir–Hinshelwood mechanisms are needed in the chain of hydrogenation steps in order to account satisfactorily for the observed ammonia concentrations, which, in the steady state, are found to reach values ~30-70% of those of N_2. The ionic composition of the plasma, which is entirely due to gas-phase processes, is the result of a competition between direct electron impact dissociation, more relevant for high electron temperatures (lower pressures), and ion-molecule chemistry, that prevails for the lower electron temperatures (higher pressures). At the lowest pressure, products from the protonation of the precursor molecules (H_3^+, N_2H^+ and NH_4^+) and other from direct ionization (H_2^+, NH_3^+) are found in comparable amounts. At the higher pressures, the ionic distribution is largely dominated by ammonium. It is found that collisions of H_3^+, NH_3^+ and N_2H^+ with the minor neutral component NH_3 are to a great extent responsible for the final prevalence of NH_4^+.

Introduction

Low pressure H_2 and N_2 plasmas have been studied both experimentally[1-11] and theoretically[7,8,10,12,13] for the last decades. The aim of the early experimental works was the synthesis of ammonia[1-4,6]. Although no detailed mechanisms were proposed, there was a general agreement that plasma-surface interactions were responsible for NH_3 production. Different experiments demonstrated that the NH_3 concentration was dependent on the materials of the electrodes[2] or on those employed to cover the walls of the plasma reactor; platinum, stainless

steel and iron being more efficient than other metals or oxides.[1,3-6] The experimental characterization of the catalysts showed that NH_x radicals were present at the surface.[3,6] The postulated mechanism involved the adsorption of excited N_2 molecules and N_2^+ ions. After their dissociation at the surface, they recombined with atomic hydrogen from the gas phase or on the surface to form successively NH_x adsorbed species. Finally, ammonia was produced and desorbed (ref. 4, 6 and references therein).

From a different perspective, theoretical studies of H_2 and N_2 plasmas, mainly focused on the modeling of gas-phase volume reactions, were developed in the nineties.[12,13] Nevertheless, surface processes had to be included subsequently by Gordiets et al.[8] in order to explain the production of ammonia and in connection with iron nitriding.[7] The model developed by these authors proposed the direct adsorption of atomic N and H (instead of dissociative adsorption of N_2 and H_2 molecules) and then, the formation of NH_x species at the surface by successive hydrogenation reactions.[8] Recent experiments have supported this reaction scheme.[10,11,14] Nevertheless, the wall material did not have influence on the ammonia synthesis. This discrepancy with previous publications was explained by the high fluxes of N and H atoms reaching the surface and passivating it. Under these conditions, the formation of ammonia took place in an additional layer on top of the passivated surface.[11] In this sense, the determination of absolute concentrations of N, H and NH_x radicals in the gas phase could help to establish the mechanism of their production and their role in the reactions at the surface.[5,10,11] The interaction of these radicals with the surface of different materials was analyzed in ref. 15 and some reaction pathways could be hypothesized in spite of the complex phenomena examined.

The characterization of these radicals and atoms in H_2/N_2 containing plasmas, and their interactions with the surface, are also of high relevance for technological applications, such as thin film growth and material processing, extended at present to the level of the nanoscale.[16,17] As an example, silicon nitride (SiN) thin films deposited by plasma-enhanced chemical vapour deposition (PECVD) are widely employed in the semiconductor industry (as a gate dielectric or passivation layer)[18] and in the photovoltaic industry[19]. Most of the deposition processes use mixtures of N_2-SiH_4 and more frequently NH_3-SiH_4, since the electron energies necessary for dissociation of ammonia are lower than for N_2. Several groups have tried to identify the main precursors for SiN deposition with differing results.[20-23] These works exemplify the complexity of the chemistry involved in film deposition and the necessity of getting further insight into the underlying mechanisms, since the properties of the films are correlated with the plasma composition and conditions[20] and have effects on the properties of the devices where these films are deposited.[24]

In nuclear fusion research, the interest is focused on the inhibition of film deposition.[25] High fluxes of hydrogen isotopes produce chemical sputtering of carbon-based materials, which leads to the formation of re-deposited (a:C-H) carbon films in regions not directly exposed to plasma.[26] Under real operation conditions, these films would have high tritium content and would pose a major problem for the handling of fusion devices.[27] Laboratory experiments for similar conditions to those present at these regions in fusion reactors have achieved the reduction of a-C:H film deposition by the introduction of N_2 in H_2/CH_4 plasmas.[28] Studies using binary and ternary mixtures of H_2, CH_4, and N_2[29,30] or NH_3,[31] provided some insight on relevant chemical processes. However, the exact inhibition mechanism is still not well understood.

The importance of surface processes in plasma chemistry is not exclusively limited to plasmas produced under laboratory conditions. Gas-phase reactions alone cannot explain the abundances of gas phase H_2, NH_3, some alcohols and other complex species in interstellar clouds, and a combination of gas-phase and surface chemistry on the ice and dust particles has been invoked to account for these abundances and for the variety of chemical species detected.[32] Research in the field is very active at the moment and theoretical efforts to improve models (see refs. 33, 34 and references therein), as well as advances in experimental studies regarding surface reactions on cosmic ice and dust[35] and closely related surface processes,[36] are growing fast, but a good understanding of the involved chemistry is still a pending issue.

On the other hand, ions play an important role in the synthesis of molecules in the interstellar medium and provide a partial picture of the free-electron abundance necessary to guarantee approximate electroneutrality. The electron density is relevant in astrophysics since it is believed to determine the rate of cloud collapse and star formation.[37] In addition, some ionic species can be used as tracers of interstellar neutrals. N_2, assumed to be the major reservoir of nitrogen in the interstellar medium,[38] lacks a permanent dipole moment and, therefore, it has no rotational transitions to be detected by radioastronomy. Then, N_2H^+ measurements are employed to estimate the concentration of N_2.[37,39] However, proton transfer from H_3^+ to N_2, which is considered the main route of N_2H^+ formation, is balanced by the destruction mechanism of dissociative electron recombination. The uncertainty in the concentrations of the charged particles involved, apart from the possible presence of additional sources and sinks of N_2H^+, results in errors as high as a factor of ten in the N_2 concentrations.[39]

In summary, experimental plasma characterization could help to improve quantitative estimations of gas phase species in H_2 and N_2 discharges, whose presence is significant in different low pressure plasmas. On the other hand, kinetic calculations can be useful to determine the relevant surface and gas-phase chemical processes and the interrelations between ionic and neutral species. In this work, we present a combined diagnostics and modeling of low

pressure H_2/(10%)N_2 plasmas generated in a hollow cathode DC reactor. The basic mechanisms leading to the observed neutral and ion distributions, as well as their relative importance in the studied pressure range, are identified and discussed.

Experimental

The experimental plasma reactor has been described elsewhere.[40,41] It consists of a grounded cylindrical stainless steel vessel (10 cm diameter, 34 cm length) and a central anode, which is pumped to a base pressure of 10^{-6} mbar by a 450 l/s turbomolecular pump and a dry pump (see Fig. 1). The reactor has additional ports for pressure gauges, windows and coupling of the experimental techniques for the plasma diagnostics (mass spectrometers for neutrals and ions, and a double Langmuir probe designed in our laboratory[42]). Molecular gases are analyzed by a quadrupole mass spectrometer with electron impact ionization, Balzers QMS200, with a secondary electron multiplier in the analog mode. The ion fluxes are detected with a Plasma Process Monitor, Balzers PPM422, which includes an electrostatic focusing system, a cylindrical mirror energy analyzer and a quadrupole mass filter, with a secondary electron multiplier in the counting mode. Both spectrometers are mounted in differentially pumped vacuum chambers, which are connected to the plasma reactor through their respective 100 μm diaphragms. The pressure during plasma measurements in both systems is ~10^{-5} Pa (base pressure in vacuum 10^{-6} Pa).

Measurements are done under continuous flow conditions. The absolute pressures of the gas precursor mixtures (measured by a capacitance manometer Leybold CTR90) are regulated by balancing the gas flow with two needle valves at the entrance (one for each gas) and a gate valve at the exit of the reactor. Mixtures of H_2 (90%) and N_2 (10%) were used for total reactor pressures of 0.8, 1, 2, 4 and 8 Pa. The ratio of both gases was fixed by measuring the intensities of the corresponding masses with the QMS. Previously, calibration of the different sensitivity of detection for each pure gas (including the global effect of the sampling diaphragm, differential pumping and QMS transmission) was done by comparison of the capacitance manometer readings at various known pressures and the quadrupole ones after background subtraction. The calibration of the mass spectrometer signals allows the measurement of the absolute concentration (or equivalently, pressure) of N_2 and H_2 before and during the discharge (where NH_3 is also observed). For experimental convenience, the NH_3 concentration is obtained by comparison with the calibration of the QMS for Ne (which has a mass close to that of ammonia), done in the same way as for N_2 and H_2, but taking into account the necessary corrections due to the different ionization cross section, the isotopic abundance of Ne and the different masses for Ne (the isotope at 20 a.m.u.) and NH_3 (the fragment at 16 a.m.u.).

Residence times of the gases in the reaction chamber, measured according to the procedure described in ref. 43, vary between 0.45 s at the lowest pressure and 0.75 s at the highest one, with typical uncertainties of 25%.

An electron gun built in our laboratory (consisting basically of a floating tungsten filament fed by a low voltage DC power supply working at 2 A, and polarized at -2000 V) is employed for the ignition of the plasma. Plasma currents $I_p \sim 150$ mA and supplied voltages in the range 300-450 V (depending on the total pressure) were sustained during the experiments.

The electron mean temperature, T_e, and total charge density, n_e, in the reactor are obtained from the analysis of the characteristic curves of the double Langmuir probe measurements in each discharge at the corresponding total pressure of the mixture. The approximation of orbital limited motion in a collision-free probe sheath is considered to be fulfilled.[44] The mean ion mass employed for the estimation of charge densities is weighted according to the ion density distributions deduced from the measurements of the Plasma Process Monitor in each case. The experimental results are displayed in Table 1.

Ion fluxes are determined by integration of the ion energy distributions recorded for each individual mass value. These energy distributions were essentially concentrated in a large and sharp maximum (full width at half maximum, FWHM ~ 2 eV) at energies very close to that of the discharge potential. Some of them also had a broad and weak tail extending to lower potentials. A calibration of the PPM transmission to the different masses, m, of the ions in the range of interest is done introducing known pressures of H_2, He, Ne, N_2 and Ar in the PPM chamber, and comparing each time the PPM signal (in this case, with the ion source switched on), weighted by the respective ionization cross section at the chosen electron energy (70 eV), with the PPM chamber pressure as determined from the reading of a Bayard-Alpert gauge with the appropriate correction factor.[30] The PPM transmission curve is proportional to $m^{-0.5}$, in agreement with other authors.[45,46] After correction by the PPM calibration, the ion fluxes coming from the discharge are multiplied by the corresponding square roots of their masses to obtain the relative ion concentrations in the plasma.

Model

A zero-order kinetic model is used to simulate the chemistry of ions and neutrals in the H_2 and N_2 plasmas. A set of time resolved coupled differential equations accounts for the different reactions taking place in the plasma glow and at the reactor walls. The solution of the system of equations describes the time evolution of the ionic and neutral species from the plasma ignition until the steady state is reached.

The input parameters of the model (whose numerical values are displayed in Table 1) are: pressures of the precursor gases (H_2 and N_2), residence times for the precursors and electron density, n_e, and temperature, T_e. All these parameters have been estimated experimentally as explained in the previous section. T_e and n_e are considered constant throughout the plasma volume for each discharge. This volume is coincident with the negative glow region and separated from the metallic walls of the reactor by an estimated sheath width[43] of 1.5-2 cm. The ion temperature is assumed to be equal to the gas (translational and rotational) temperature (300 K),[42,47] which coincides also with the temperature of the reactor walls.

The different chemical reactions included in the model, together with their corresponding rate coefficients, are listed in Table 2 (gas phase chemistry) and Table 3 (surface chemistry). The gas phase processes considered are electron impact ionization (I_1-I_{12}), electron impact dissociation (D_1-D_7), electron impact neutralization (N_1-N_{12}) and ion-molecule reactions (T_1-T_{25}). The surface processes comprise ion neutralization at the reactor walls (K_1-K_{10}) and heterogeneous reactions among the neutral species (W_1-W_{15}).

Electron impact ionization rate coefficients for H and H_2 and electron impact dissociation for H_2 have been calculated by fitting the up-going post-threshold part of the measured cross sections to a line-of-centers functionality[48] (see Table 2 for references). This functionality leads to a simple Arrhenius like expression for the temperature dependence of the rate coefficient. Following an analogous procedure and using the recommended cross section for the electron-impact dissociation of N_2 by Cosby[49], the corresponding rate coefficient has been estimated. According to ref. 49, predissociation to form $N(^2D) + N(^4S)$ products is the dominant dissociation mechanism. The contribution of $N(^4S) + N(^4S)$ and $N(^2P) + N(^4S)$ minor channels cannot be totally excluded though. For simplicity, the model considers only one kind of nitrogen atoms, labeled N, irrespective of their initial electronic state. The electron impact dissociation rate coefficient for NH, NH_2 and NH_3 is expressed by the same type of line-of-centers functionality. The threshold energies for the relevant dissociative states have been taken from photodissociation experiments and from calculations.[50-53] The pre-exponential factors have been estimated for consistency with the present data.

The free plasma electrons are assumed to follow a Maxwellian-like energy distribution. Deviations from a Maxwellian behaviour in N_2 containing plasmas, due to a coupling between vibrational excitation and the electron energy distribution function (EEDF), has been analyzed in depth in the past,[12,54] and it has been shown that in plasmas rich in H_2, the deviation from a Maxwell distribution is not very pronounced.[12] Given the relatively low concentration of N_2 in our plasmas and the measured electron temperature T_e (3-4 eV), we believe that the Maxwellian EEDF is still a reasonable approximation.

The absolute partial rate coefficients for electron impact ionization of the various N_x and NH_x species are expressed as polynomial expansions in T_e. These rate coefficients were obtained by averaging the corresponding ionization cross sections from the cited literature sources over the assumed Maxwell distribution of electron energies. The cross-sections for ammonia and for the radicals NH and NH_2 were reported by two groups.[55,56] Given the insensitivity of electron impact ionization to isotopic substitution, both groups used deuterated variants in their measurements for experimental convenience. We have selected the results of ref. 58 because they lead to a better agreement with our measurements.

Excited atoms and molecules can be formed in H_2/N_2 plasmas of different kinds, mostly by electron impact or in surface processes (see for instance[8,13,14,57-59] and references therein). Their influence on the chemistry of H_2 and N_2 DC discharges of variable concentrations has been studied in detail in the model of Gordiets et al.[8,13] For the low pressures of our discharges and for the dimensions and characteristics of our reactor, which favor neutral chemistry at the metallic walls, the contribution of excited species to the global chemistry is expected to be small, given their comparatively low concentration and relatively moderate rate coefficients for reaction with major plasma species.[8,13] Consequently, we have not included excited species in the model. Binary gas-phase reactions between ground state neutral species have not been considered either, due to their low probabilities at room temperature (see ref. 13 and references therein). Three-body processes can be also ignored at the low pressures of our discharges.

Rate coefficients for the relevant ion-neutral reactions (T_1-T_{25}) at a gas temperature of 300K have been taken from the compilation by Anicich.[60] The rate coefficients for the recombination of electrons and positive ions (N_1-N_{12}), taken from various literature sources, are also included in Table 2. Negative hydrogen ions, H^-, are often considered in the modeling of H_2 containing plasmas, but again, as discussed in ref. 61, their concentration is expected to be negligible for the conditions of our discharges.[62]

The rate coefficients (K_1-K_{10}) for the neutralization of ions at the wall are obtained by considering that the net ion generation in the gas phase (difference between the total ion concentration produced by ionization, $\sum_{j=1}^{15} c_j [X_j] n_e$ and destroyed by neutralization, $\sum_{m=1}^{12} c_m' [Z_m] n_e$) must be balanced by the total ion flux to the cathode wall, in order to meet the electroneutrality condition[41]

$$K_i = \tau_i^{-1} = \frac{\sum_{j=1}^{15} c_j [X_j] n_e - \sum_{m=1}^{12} c_m' [Z_m] n_e}{\sqrt{m_i} \cdot \left(\sum_{l=1}^{10} \frac{[Z_l]}{\sqrt{m_l}} \right)} \quad (1)$$

where $[X_j]$ refers to the concentration of the neutrals and $[Z_m]$ and $[Z_l]$, to the ionic species. The loss rate of a given ion to the reactor walls is proportional to its mobility, and thus inversely proportional to the square root of its mass[63] $\sqrt{m_i}$.

Regarding heterogeneous processes at the walls of the reactor, some general approximations have been introduced: the adsorption is Langmuirian, i.e., gas phase species can only adsorb on free surface sites until the surface is fully covered by adsorbates (monolayer adsorption), all the surface sites are treated as identical and the adsorbate-adsorbate interactions are neglected. Surface modifications and/or solubility of gases in the bulk have not been considered of relevance for the kinetics of ammonia production. This assumption is based on surface science studies and high-pressure catalysis modeling (see ref. 64 and references therein).

The effect of adsorption on the concentrations of the atomic and radical gas phase species denoted by [X] (where [X] in cm^{-3} refers to H, N, NH and NH_2) is described by the following rate equation:

$$\frac{d[X(s)]}{dt} = -w_{ads} \cdot S_F \cdot [X] = -\frac{1}{\tau_{ads} \cdot S_T} \cdot S_F \cdot [X] \quad (2)$$

where w_{ads} is the rate coefficient, S_F the free surface site density and S_T the total surface site density, for which the conventional 10^{15} cm^{-2} value[65] has been assumed. The free surface site density is expressed as $S_F = S_T - \sum [X(s)]$, where [X(s)] indicates the density of atoms or radicals adsorbed on the surface (cm^{-2}). τ_{ads} is a decay time for the particle density in the gas phase due to diffusion and adsorption at the reactor's wall, which is given by:

$$\tau_{ads} = \frac{\Lambda^2}{D} + \frac{V}{A} \cdot \frac{4 \cdot \left(1 - \frac{1}{2}\gamma_{ads}\right)}{\bar{v} \cdot \gamma_{ads}} \quad (3)$$

where we follow the formulation of Chantry.[66,67] Λ is the diffusion length, D, the diffusion coefficient, $\bar{v}$ is the thermal velocity of atoms and radicals and V/A, the volume-area ratio of the reactor.

The value of the sticking coefficient, γ_{ads}, for atomic H, N and the radicals NH and NH_2 is selected to be 1 on metallic wall reactors, since the sticking probability of atoms and radicals

is known to be high on transition metals.[63] On the contrary, N_2 and H_2 dissociative adsorption is neglected under plasma conditions, (for example, the dissociative adsorption sticking coefficient of N_2 on Fe surfaces near room temperature is very low[68], ~10^{-6}, and ≤ 0.1 for H_2[69]).

The evolution of adsorbed species, X(s), is defined by:

$$\frac{d[X(s)]}{dt} = w_{ads} \cdot \frac{V}{A} \cdot S_F \cdot [X] = \frac{1}{\tau_{ads} \cdot S_T} \cdot \frac{V}{A} \cdot S_F \cdot [X] \qquad (4)$$

which is formally analogous to equation (2). The possibility of desorption of X_s depends on its binding energy to the surface, usually ≥ 1eV for chemisorbed species.[70] Implicitly, we assume that atoms and radicals are chemisorbed on the metallic reactor walls. Therefore, the spontaneous desorption of H(s) and N(s) atoms, and NH(s) and NH_2(s) radicals, is highly improbable, and desorption reactions have not been included in the model (see Table 3).

H_2 and N_2 can be formed by surface processes. In principle, both Eley-Rideal and Langmuir-Hinshelwood mechanisms are possible. The first process occurs by abstraction of one H(s)/N(s) atom by an incoming H/N gas phase atom, and the Langmuir-Hinshelwood mechanism, by reaction between two adsorbed atoms, i.e., H(s) + H(s) → H_2 + 2F_s where F_s represents a free surface site. However, in a previous work[61] the kinetic model showed that only ER recombination was relevant for the formation of H_2, D_2 and HD from H_2 and D_2 discharges in the same reactor used in the present study. The comparison of model calculations and measurements led to the conclusion that the activation energy for LH reaction was too high for those discharges. In our present work, with mixtures containing 90% H_2, a basically similar behavior is expected. In the case of N_2, the LH mechanism is even less important, since the higher activation barriers for diffusion[71,72] determine a lower surface mobility of nitrogen atoms, as compared with hydrogen atoms. In fact, surface kinetic simulations predict higher activation energies for the formation of N_2 than for that of H_2.[73] The previous considerations indicate that the production of H_2 and N_2 molecules takes place essentially through the Eley-Rideal reactions W_2 and W_4. The rate of formation of [XY] (in this case X≡Y) is given by:

$$\frac{d[XY]}{dt} = w_{ER_{XY}} \cdot [X][Y(s)] = \frac{1}{\tau_{ER_{XY}} \cdot S_T} \cdot [X] \cdot [Y(s)] \qquad (5)$$

$w_{ER_{XY}}$ is the rate coefficient and $\gamma_{ER_{XY}}$ is formulated as before :

$$\tau_{ER_{XY}} = \frac{\Lambda^2}{D} + \frac{V}{A} \cdot \frac{4 \cdot \left(1 - \frac{1}{2}\gamma_{ER_{XY}}\right)}{\bar{v} \cdot \gamma_{ER_{XY}}} \qquad (6)$$

where the γ_{ads} coefficient of equation (3) is substituted for the ER surface coefficient $\gamma_{ER_{XY}}$. The value of $\gamma_{ER_{XY}}$ selected for H_2 is 1.5×10^{-3} (taken from ref. 61) and a value of 6×10^{-3} is estimated for N_2.

The production of NH_3 is assumed to take place by the successive hydrogenation of adsorbed nitrogen atoms and nitrogen containing radicals at the surface of the stainless-steel reactor walls. In fact, the gas phase volume reactions alone are not able to produce ammonia in detectable amounts in our case, in agreement with previous works[8,59]. The proposed reaction scheme (W_5-W_{15}) at the surface, developed in accordance with those already presented by other authors[8,11], is shown in Table 3. A combination of Eley-Rideal (ER) (understood in the sense of incoming gas phase species directly reacting with adsorbed ones, independently of the immediate desorption or not of the product) and Langmuir-Hinshelwood (LH) reactions produces adsorbed NH_x radicals in additive steps until NH_3 is formed and desorbed to the gas phase. The desorption step is assumed to be immediate and has been omitted following refs. 8, 10 and 11. The abrupt drop of the NH_3 signal in the quadrupole mass spectrometer after switching off the discharge supports this last assumption. Even so, some tests with the model have been done including a desorption step for NH_3 (with barriers for desorption ≤ 0.5 eV[71]). The steady-state is attained later but the concentrations are basically unaffected and the surface coverage of $NH_3(s)$ is negligible in comparison with the rest of the adsorbed species. The LH reaction H(s) + N(s) $\rightarrow$ NH(s) has been excluded since the energetic barrier for this process is moderately high[71] and difficult to overcome at the temperature of our experiments. Therefore, it is clearly less efficient than the E-R reactions (W_7-W_8) to produce NH(s) radicals.

The rate of adsorbed NH_x radicals production by means of the ER reactions W_7-W_{10} is expressed as:

$$\frac{d[XY(s)]}{dt} = w_{ER_{XY(s)}} \cdot \frac{V}{A} \cdot [X][Y(s)] = \frac{1}{\tau_{ER_{XY(s)}} \cdot S_T} \cdot \frac{V}{A} \cdot [X] \cdot [Y(s)] \qquad (7)$$

where Y(s) stands for the atom or radical adsorbed at the surface, X, for the impinging atom, and XY(s), for the adsorbed radical after reaction. $w_{ER_{XY(s)}}$ is the rate coefficient for these processes and $\tau_{ER_{XY(s)}}$, the characteristic time for these ER reactions, which is given by:

$$\tau_{ER_{XY(s)}} = \frac{\Lambda^2}{D} + \frac{V}{A} \cdot \frac{4 \cdot \left(1 - \frac{1}{2}\gamma_{ER_{XY}(s)}\right)}{\bar{v} \cdot \gamma_{ER_{XY(s)}}} \qquad (8)$$

In addition to the ER mechanism just discussed, the adsorbed radical $NH_2(s)$ can be formed at the surface of the metallic walls by a LH mechanism (reaction W_{11}). The corresponding rate equation can be expressed as[8,74]:

$$\frac{d[XY(s)]}{dt} = w_{LH} \cdot [X(s)][Y(s)] = \frac{\nu}{4 \cdot S_T} \cdot e^{-\left(\frac{E_d + E_a}{k_B T_w}\right)} \cdot [X(s)] \cdot [Y(s)] \qquad (9)$$

where we consider that the adsorbed species can migrate by surface diffusion: ν is the surface diffusional jump frequency (whose value is assumed to be[72] $\approx 10^{13}$ s^{-1}) and E_d, the activation energy for diffusion (an assumed value of ~0.2 eV, characteristic of chemisorbed H atoms on Fe surfaces[72]). E_a stands for the activation energy of the chemical process. The values of E_a used for the model are 0.3 eV for reaction W_{11} (compatible with surface studies for chemisorbed species[71,73]). T_w is the temperature at the reactor wall (~300 K) and k_B is the Boltzmann constant.

The rate of formation of ammonia by the ER reactions W_{12}-W_{14} is also expressed by the equations (4) and (5) taking into account that X refers not only to an atom, but also to a radical or stable molecule in the gas phase. Y(s) corresponds to an adsorbed atom or radical.

Finally, the rate expression for the production of NH_3 by the LH reaction W_{15} is similar to (9):

$$\frac{d[XY]}{dt} = w_{LH} \cdot \frac{A}{V}[X(s)][Y(s)] = \frac{\nu}{4 \cdot S_T} \cdot e^{-\left(\frac{E_d + E_a}{k_B T_w}\right)} \cdot \frac{A}{V}[X(s)] \cdot [Y(s)] \qquad (10)$$

but XY is a desorbed gas phase product instead of an adsorbed one. In this case, the value of activation energy E_a is 0.2 eV. The rest of parameters are defined as before (with the same numerical values).

The values of $\gamma_{ER_{XY(s)}}$ employed in the model are included in Table 3. These values, which as far as we know are not available in the literature, have been chosen for a best global agreement with the extensive set of data measured in this work over the whole range of pressures investigated. In accordance with intuitive expectations and for consistency with the results of Jauberteau et al.[10], the γ_{ER} coefficient for reaction W_{14}, which implies gas phase H_2 molecules, has been assumed to be significantly smaller than those involving gas phase atoms or radicals.

Results and discussion

The experimental measurements of the present work demonstrate the high efficiency of the investigated discharges for the generation of NH_3 and of its ionic derivative NH_4^+. The following discussion is centered on the analysis of the relative relevance of the various mechanisms responsible for the appearance of these species under the different circumstances considered. The efficient generation of ammonia in these low temperature plasmas, suggests the possibility of substituting the hazardous NH_3 by N_2 as fuel gas for discharges in processing applications in various fields (nanotechnology, production of nitride films…).

The experimental relative concentrations of neutral species measured at three different pressures (0.8, 2 and 8 Pa) are shown in Figure 2, together with the model calculations. The results obtained at 1 and 4 Pa (not displayed) show an intermediate behaviour. The concentrations of the calculated and measured stable molecules (H_2, N_2 and NH_3) are put to scale for comparison. Apart from the precursor gases, NH_3 is detected in significant amounts, with a higher relative concentration at the lowest pressure. In addition, the figure includes the atomic (H and N) and radical (NH and NH_2) distributions given by the model. Although these species have not been experimentally detected, the relatively high atomic H concentrations are consistent with previous results from our group[40] and appreciable concentrations of the NH and NH_2 radicals have also been observed by other groups in H_2/N_2 discharges.[5,10] In our case, gas phase dissociation of ammonia is the main source of NH and NH_2 radicals.

The steady-state concentrations of the neutral species for each pressure are the result of a complex balance between dissociation by electron impact of the stable molecules (not only of the H_2 and N_2 precursors but also of ammonia) and radicals, and surface generation of the stable species, predominantly NH_3 but also H_2 and N_2 (see Table 3). The precursor gases are largely recycled before leaving the reactor due to the relatively long residence times (between ~0.45 and 0.75 s). The increase in NH_3 concentration at 8 Pa, which could be intuitively expected due to the higher residence time at this pressure, is basically compensated by a slight increase of the plasma volume (i.e., a smaller sheath width that is estimated to change from 2 to 1.5 cm with increasing pressure[43,63]), which favors NH_3 dissociation. NH_3 formation is triggered by the supply of atomic H and N to the surface, which depends on an efficient dissociation of H_2 and N_2. The efficiency grows substantially with increasing electron temperature, T_e, as can be observed in Figure 3 a, where the rate coefficients for electron impact dissociation of the various neutrals present in the plasma (reactions D_1-D_7) are displayed over the range of electron temperatures of interest for our experiments (note that the rate coefficient of reaction D_4 is equal to that of D_5). Since the dissociation rate of N_2 is the lowest of all neutral species and its proportion in the mixture is only 10%, the adequate supply of N atoms to the reactor walls, regulated by T_e, will be an important control parameter for the production of ammonia at the

surface. It is worth noting that the dissociation of the NH_x species is very efficient already at low T_e but less sensitive than that of H_2 and N_2 to a change in T_e.

Further insight into the interconnected gas phase and surface chemistry can be gained by analyzing the model steady-state concentrations of the most relevant neutral species as a function of electron temperature. Calculated results at 2 Pa are displayed in Figure 4 for gas phase molecules and atoms (a) adsorbed species (except for NH_2(s), $<10^{12}$ cm^{-2} anywhere) (b) and the most representative surface production terms (c).

The minimum concentration of NH_3 is predicted at the lowest T_e (2 eV) due to a limited supply of atomic N; but even for this electron temperature, a significant amount of NH_3 is already produced, mainly through reactions W_{13} and W_{15}. Reaction W_{12} represents a minor contribution to ammonia formation at any pressure and is not shown in the figure. Because H_2 constitutes 90% of the precursor mixture and its dissociation is more efficient than the dissociation of N_2, H is the main atomic or radical species in the gas phase and at the surface. This second circumstance allows not only the formation of NH_3 but also the formation of H_2 via reaction W_2. As a consequence, part of the adsorbed H is lost for the generation of ammonia and it is recovered as one of the precursor species. However, between 2.5 and 3 eV, the dissociation of N_2 starts to be more efficient, N adsorption is more relevant than before, reaction W_8 gains in importance and, under steady-state conditions, an enriched N(s) surface produces NH_3 mainly through reactions W_{14} and W_{15}. At the same time, the formation of H_2 via W_2 is inhibited and the production of N_2 via W_4 too, since most of the atomic N is at the surface or takes part in ammonia generation. The most favorable situation for NH_3 production corresponds to the conditions in which atomic gas-phase concentrations are drastically reduced and the surface is preferentially covered with atomic N. These conditions are not fulfilled beyond 3 eV, since gas phase dissociation is significant, leading especially to atomic H. The excess of atomic H reverts to a prevailing H(s) covered surface and the production of H_2 at the surface grows substantially. With growing T_e, the dissociation of N_2 is also favored and reaction W_4 produces also more N_2. These processes are responsible for the small upturn in both molecular concentrations near 3.1 eV. At higher T_e, the dissociation of molecular species is so efficient that their steady-state concentrations drop in spite of the more efficient surface production.

As a consequence of the complex balance between electron impact dissociation and the various surface processes, the concentration of NH_3 is predicted to be maximized in the plasma over a given T_e range that depends on pressure. Figure 5 shows the evolution of the relative NH_3 concentration as a function of T_e for the three pressures considered, together with the experimental measurements corresponding to the actual discharges investigated. Note that just one experimental point can be measured at each pressure with our experimental set-up. This

point corresponds to the condition where the Te value adjusts itself automatically for each pressure. The measured data are certainly consistent with the calculations, but they should not be viewed as a rigorous proof of the predictions, which are not restricted to a single electronic temperature, but extend over a T_e range. In this respect, the figure depicts basically model results. As can be seen, the interval of maximal NH_3 concentration is narrow at the higher pressures, but becomes broad, with a gentle decline toward higher T_e, for 0.8 Pa. The experimental points for the 2 Pa and 8 Pa discharges turn out to be just beyond their respective maxima, which end in an abrupt fall. The point for the 0.8 Pa discharge is also past the maximum, but its value is not much lower, since it is placed on the gentle down-going slope. In retrospect it is not surprising that the maximum relative concentration of ammonia was measured for the lower pressure, since in this case, NH_3 production is favored over a much wider T_e range.

As indicated above, both LH and ER mechanisms have been considered in a combined reaction scheme for the synthesis of ammonia on the metallic surface, in accordance with previous literature works[8,14]. However, given the high flow of atoms to the wall characteristic of our low pressure plasmas, it is worth investigating whether a scheme based purely on ER reactions could account for our experimental data. To these end we have performed additional simulations with the model. The results are represented in Figure 6 for the 0.8 Pa discharge, i.e., the one with the lowest pressure and most sensitive to surface processes. A direct elimination of the two LH processes included in the model (reactions W_{11} and W_{15}) without changing the γ_{ER} coefficients leads to a too low NH_3 production and to a distortion in the predicted concentrations of H_2 and N_2 which are overestimated and underestimated respectively (black bars). In order to recover the agreement with experimental results without the LH reactions, the γ_{ER} coefficients must be raised significantly, as shown by the stripped bars in the figure that correspond to a ten-fold increase in the value of γ_{ER} for nitrogen recombination and to a five-fold increase in the γ_{ER} values for all reactions involving NH_x species. These values are deemed unrealistically high and are not suitable for the higher pressures. Our results support thus the prevalent view stressing that LH reactions are also of relevance for the heterogeneous synthesis of ammonia in this type of plasmas.

The model analysis of the plasma kinetics described thus far outlines the basic processes responsible for the observed composition of neutral species and underlines the strong interconnection between gas-phase and surface chemistry and the crucial influence of electron temperature. Specifically, the production of NH_3 has been found to depend very sensitively on the delicate balance between formation and destruction of the NH_x intermediates implied. The model provides in principle a good global picture of the steady state plasma chemistry, but it

also has obvious limitations, since it relies on a series of assumptions about the number of surface sites or surface reaction parameters. In the absence of in situ surface characterization, which is beyond our experimental capabilities, the predictions about coverage by the distinct species cannot be directly verified. Apart from wall neutralization, the model neglects ionic interactions with the surface and it does not consider ionic effects on the surface chemistry or a possible surface modification by electron bombardment. The reproducibility of the experiments suggests, however, that the surface is not appreciably modified by the studied discharges.

Figure 7 shows the measured ion distributions at 0.8, 2 and 8 Pa (as in the case of neutrals, the results at 1 and 4 Pa display intermediate behaviors). At the lowest pressure, the relative concentrations of H_2^+, H_3^+, NH_3^+, NH_4^+ and N_2H^+ have similar values; but with increasing pressure, the concentration of NH_4^+ grows progressively and largely dominates the ionic distribution at 8 Pa. The relative ionic concentrations resulting from the model calculations are also displayed for comparison. The global evolution with pressure is satisfactorily reproduced by the model although some discrepancies are observed (see below). As found previously in plasmas of other gas mixtures[75], the overall ion results can be explained mainly by the decrease of the electron temperature T_e at higher pressures. NH_4^+ together with H_3^+ and N_2H^+ are formed exclusively by ion-neutral gas phase reactions (see Table 2). In contrast, the rest of the ions can also be generated in significant amounts by direct ionization (in fact, for H_2^+ and N_2^+ this is the only way). This channel tends to be preferential for high T_e, since production by some of the ion-molecule reactions T_1-T_{25} is often compensated by destruction via other reactions in the group. The rate coefficients of the most relevant ionization reactions (I_3, I_6, I_{11} and I_{12}) as a function of the electron temperature T_e are displayed in Figure 3 b. At 8 Pa, T_e is slightly lower than 3 eV and the rate coefficients for electron impact ionization are smaller than those for the ion-molecule reactions. Under these circumstances, the ion distributions are determined to a large extent by ion-molecule chemistry, which leads preferentially to NH_4^+ as soon as NH_3 is present in appreciable concentrations (the ammonium ion does not have destruction channels in the gas phase and is essentially lost through wall neutralization). However, at 0.8 Pa, the electron temperature reaches 4 eV and the rate coefficients for direct ionization, notably those for NH_x species, approach those for ion-molecule reactions. Consequently both types of processes compete and a more uniform distribution of ionic concentrations is observed. The relative concentration of NH_4^+ decreases at 0.8 Pa with respect to higher pressures, whereas the proportions of the rest of the ions, especially NH_3^+ and NH_2^+ grow appreciably. The relative concentration growth is also found, to a smaller extent, for H_3^+ and N_2H^+ (which are not formed by direct electron impact ionization), due to the larger availability of their primary ionic precursors.

The key role played by electron temperature in the ion distribution is further illustrated in Figure 8, which shows the calculated evolution of molecular ions with T_e in the 2 Pa discharge. For this simulation, plasma volume and electron density are kept constant. A very similar qualitative behavior, not shown for brevity, is also obtained for the other two pressures investigated. For the lowest electron temperature, the rates of ion production by electron impact are low (see Fig. 3b) and, as just mentioned, the generated ions are preferentially transformed into NH_4^+ through the chemical network listed in table 2 (reactions T_1-T_{25}). Note that the NH_4^+ concentrations are divided by a factor of two in Fig. 8. With increasing T_e the concentration of NH_4^+ decreases sharply and those of the other ions increase, giving rise to more uniform distributions. Between T_e~4 and 5 eV the major ion is NH_3^+, with a significant contribution from direct ionization. Beyond 5 eV, the H_2^+ ion, formed exclusively in the electron impact ionization of H_2, becomes dominant. Between 2 and 3 eV, the maximum in the concentration of NH_3 as a function of T_e commented on above is clearly imprinted in the curves of the various ions implied in NH_3 chemistry. Reactions T_8, T_{22} and T_{25} lead to a relative growth of NH_4^+ and to a concomitant decrease of H_3^+, NH_3^+ and N_2H^+ in clear correspondence with the NH_3 maximum shown in figures 4 and 5.

Although the model predicts well the global relative experimental ionic concentrations at a given pressure and their changes as the pressure is modified, there are some discrepancies between the experimental concentrations of some ions and the calculated ones. NH_2^+ and NH_3^+ are overestimated by the model and H_2^+ and H_3^+ are underestimated. These differences are present in all cases, but they are more evident at the highest pressures. The reasons for these discrepancies are not clear, especially considering that ionic chemistry is strictly restricted to the gas phase and is not plagued by the uncertainties commented on above for surface reactivity. Specifically, consistent values for the relevant electron impact ionization cross sections are available and the rate coefficients for the main gas phase sinks and sources of the various ions seem well established in the literature (see literature sources in Table 2 and the references cited in them). Sheath collisions, leading to additional reactions or charge transfer, not considered in the model, could contribute to explain the differences between the experimental data and the model results, but they are very difficult to evaluate due to the scarcity of data on cross sections for molecular ions over the required energy range (up to 300-400 eV). The comparatively low pressure of the experiments and the analysis of the ion energy distributions reaching the cathode[43] suggest that the measurements should not be significantly perturbed by collisions in the plasma sheath, but some distortion of the measurements cannot be entirely ruled out (see references[75,76] for more detailed comments on possible sheath effects). The assumption of a Maxwell distribution of electron energies and the neglect of internally excited species in the

model calculations may also contribute to the observed discrepancies between measurements and simulations.

Before closing this section, it is worth noting that the efficient transformation of N_2H^+ into NH_4^+ in the presence of NH_3 reflected in the results of this work can have implications for astrophysics, mainly in protostellar regions, where temperatures can be high enough to evaporate NH_3 from the dust grains. The evaporated NH_3 would then deplete N_2H^+ directly, through reaction T_{25}, and indirectly by destroying its precursors H_2^+ and H_3^+ through reactions T_4 and T_8. Under circumstances, this NH_3 chemistry could modify the balance between N_2H^+ formation through proton transfer from H_3^+ to N_2 (T_9) and the destruction mechanism of dissociative electron recombination (N_{12}) assumed in estimates of molecular N_2 concentrations.[39]

Summary and conclusions

H_2-N_2 plasmas with a low content of N_2 in the precursor gas mixture (~10%) generated in a hollow cathode DC reactor have been characterized experimentally using mass spectrometry, for the measurement of neutrals and ion concentrations and a double Langmuir probe, for the estimation of electron temperatures and densities. Apart from the precursors, ammonia is detected in appreciable concentrations, comparable to that of N_2 at the lowest pressure. A simple zero order kinetic model which couples gas-phase and heterogeneous chemistry, reproduces the global composition of the plasmas over the whole range of pressure experimentally studied. A detailed analysis based on the results of the model has allowed the identification of the main processes determining the observed neutral and ion distributions and their evolution with discharge pressure.

Ammonia is formed at the surface of the metallic reactor walls by the successive hydrogenation of atomic nitrogen and nitrogen containing radicals. Both Eley-Rideal and Langmuir-Hinshelwood mechanisms are necessary to account for the measured distributions of neutrals. At the lowest pressure, the gas phase dissociation of N_2, which is controlled mainly by the electron temperature, supplies an adequate flux of N atoms to the walls to favor ammonia production. A feedback mechanism allows the enrichment of the surface in atomic N which, at the same time, reduces drastically H_2 formation at the surface via an Eley-Rideal mechanism and guarantees an efficient NH_3 generation. As a result, the concentration of NH_3 approaches that of N_2. With growing pressure, the plasma conditions provide a relatively high H atomic content in the gas-phase and lead to a preferentially H-covered surface, which forms not only ammonia but also molecular H_2 (and to lesser extent N_2). As a consequence, the presence of NH_3 in the relative concentrations of neutral species decreases.

The plasma ion distributions, produced exclusively in the gas phase, are largely influenced by variations in the electron temperature. At lower pressures and higher electron temperatures, the rates of electron impact ionization compete with those of ion molecule chemistry. The resulting ion distribution is relatively uniform, with similar concentrations of several ions. However, at higher pressures and lower electron temperatures, ion-molecule processes control the chemistry and the protonation reactions result ultimately in a distribution of ionic species with a marked NH_4^+ predominance. The strong prevalence of NH_4^+ in the distribution is a direct result of the ion molecule chemistry of NH_3, which mediates the generation of ammonium ions at the expense of H_3^+ and N_2H^+. This intertwined reactivity of the three protonated ions should be considered in the estimations of molecular N_2 densities in astrochemistry, which are mostly based on N_2H^+ measurements, if ammonia is present in appreciable amounts in the gas phase.

Acknowledgments

This work has been funded by the MICINN of Spain under projects FIS2010-16455 and CSD2009-00038. EC acknowledges also funding from the JdC program of the MICINN. We are indebted to J. M. Castillo, M. A. Moreno, D. Pérez and J. Rodríguez for technical support.

Figure captions

Figure 1. Experimental setup

Figure 2. Experimental (grey bars) measurements and model calculations (black bars) of the relative concentrations of neutral species in the H_2/(10%)N_2 mixture at (a) 0.8 Pa, (b) 2 Pa and (c) 8 Pa. The experimental and theoretical distributions have been put to scale by normalizing the sum of the signals corresponding to masses 2, 28 and 16, for which measurements are available.

Figure 3. (a) Dissociation rate coefficients of the stable molecules (H_2, N_2 and NH_3) as well as radical species (NH and NH_2) as a function of the electron temperature (T_e). (b) Ionization rate coefficients of H_2, N_2 and NH_3 as a function of the electron temperature (T_e). See text and table 2.

Figure 4. Calculated variations of the steady-state concentrations for the most significant gas phase neutrals (a), adsorbed species (b) and surface production terms (c) with electron temperature (T_e) at 2 Pa. The labels in (c) have the same nomenclature used for the surface reactions of Table 3. They indicate the final product formed too. LH and ER stand for Langmuir-Hinshelwood and Eley-Rideal mechanisms, respectively. The best fitting to the experimental results corresponds to a T_e=3.1 eV. See text for further explanations.

Figure 5. Calculated relative NH_3 concentration as a function of T_e for 0.8, 2 and 8 Pa. The dots with error bars indicate the experimental values.

Figure 6. Experimental and calculated neutral species (only stable molecules are shown) by employing exclusively an Eley-Rideal model for surface reactivity (i.e. excluding W_{11} and W_{15}) with the same γ_{ER} coefficients of the complete model (1), and with a ten-fold increase in the value of γ_{ER} for nitrogen recombination and a five-fold increase in the γ_{ER} values for all reactions involving NH_x species (2). See text for further details.

Figure 7. Measured (grey bars) and calculated (black bars) ion distributions for plasmas with a H_2/(10%)N_2 precursor mixture at (a) 0.8 Pa, (b) 2 Pa and (c) 8 Pa. The sum of the signals for each case has been normalized to one.

Figure 8. Changes of the calculated ionic distribution with electron temperature (T_e) in the 2 Pa discharge. Note that the displayed NH_4^+ concentration is divided by a factor of two.

Figure 1

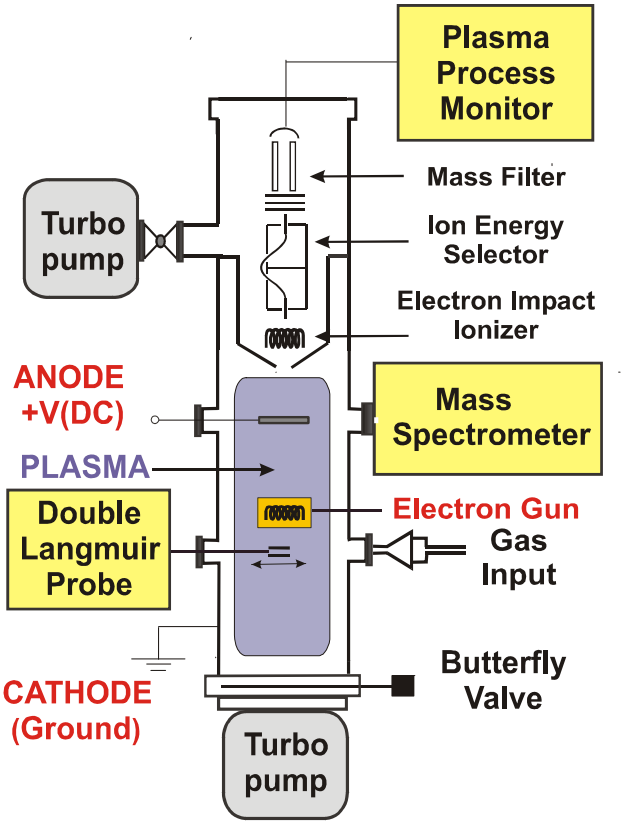
Plasma Process Monitor
Mass Filter
Ion Energy Selector
Electron Impact Ionizer
Turbo pump
ANODE +V(DC)
Mass Spectrometer
PLASMA
Double Langmuir Probe
Electron Gun
Gas Input
Butterfly Valve
CATHODE (Ground)
Turbo pump

Figure 2

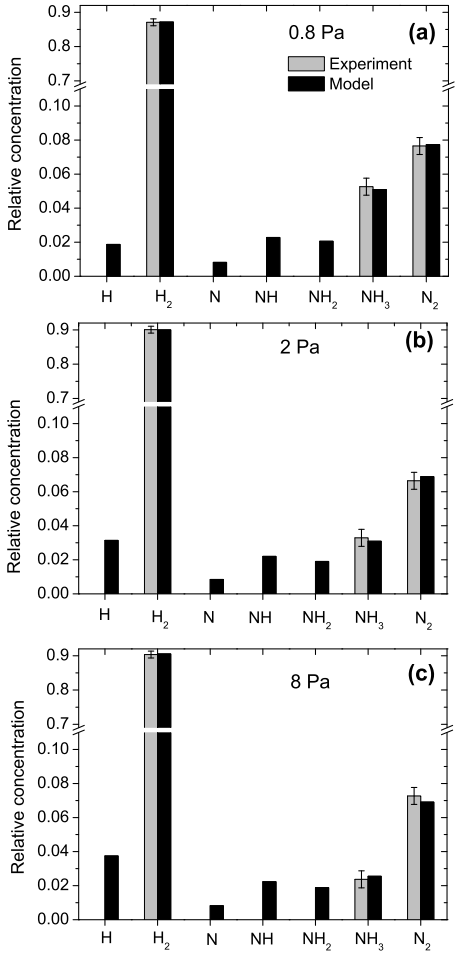

Figure 3

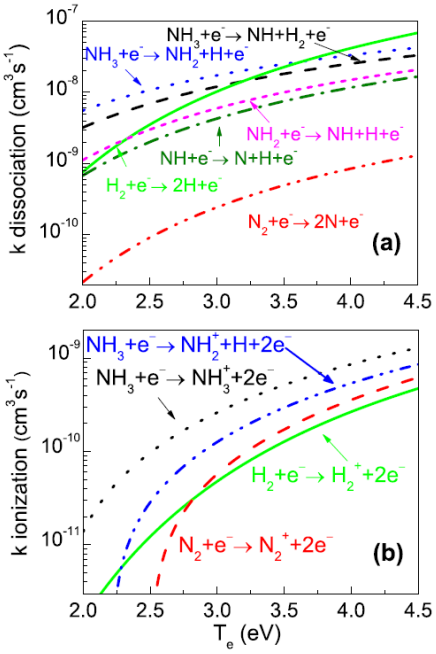

Figure 4

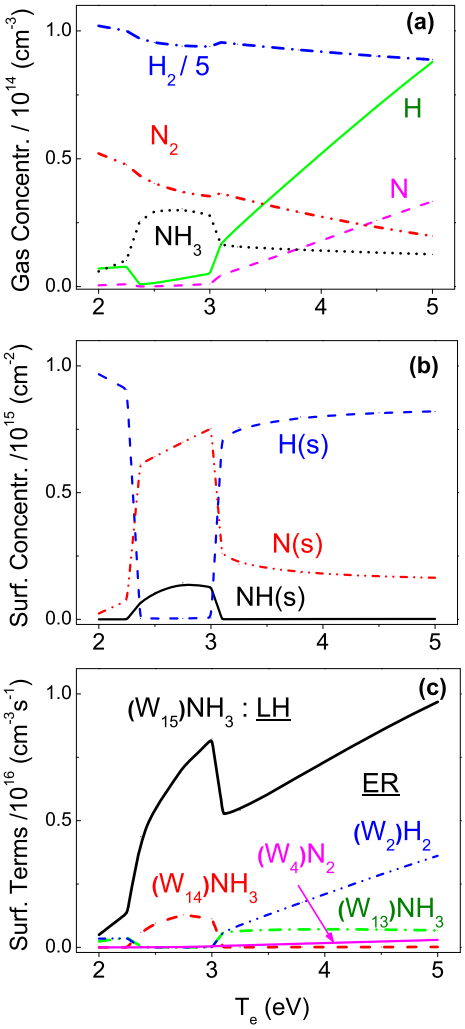

Figure 5

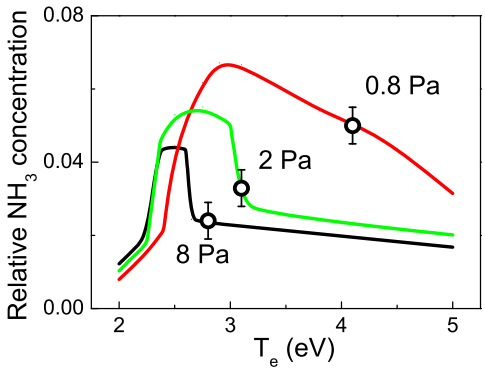

Figure 6

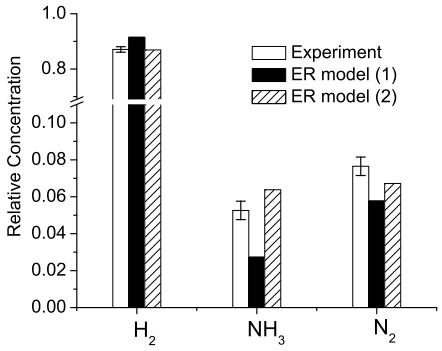

Figure 7

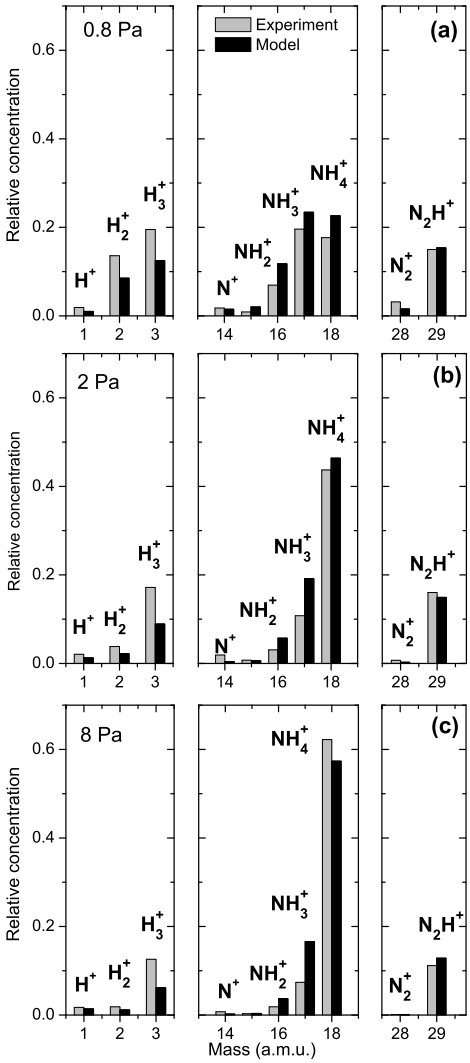

Table 1. Electron temperatures (T_e) and densities (N_e) obtained experimentally by the Langmuir probe and adjusted to the best fittings to neutral and ion concentrations in the model at different pressures, together with the corresponding residence times (t_r).

Pressure (Pa)	T_e (eV, experiment)	T_e (eV, model)	N_e (cm^{-3}, experiment)	N_e (cm^{-3}, model)	t_r (s, experiment)	t_r (s, model)
0.8	3.8 ± 0.5	4.15	2.6 ± 0.5	2.3	0.45 ± 0.15	0.43
2	3.4 ± 0.5	3.1	3.5 ± 0.5	3.6	0.55 ± 0.15	0.53
8	3.1 ± 0.5	2.8	2.8 ± 0.5	3.3	0.75 ± 0.15	0.61

Table 2. Homogeneous reactions

	Process	Rate coefficient ($cm^3 s^{-1}$)	Reference
	Electron impact ionization		
I_1	$N + e \rightarrow N^+ + 2e$	$1.26\times10^{-10}xT_e - 1.72x10^{-10}\,xT_e^2 + 6.51\times10^{-11}xT_e^3 - 5.75x10^{-12}xT_e^4 + 1.71\times10^{-13}xT_e^5$	77
I_2	$N_2 + e \rightarrow N^+ + N + 2e$	$-5.68\times10^{-12}xT_e + 8.57x10^{-12}\,xT_e^2 - 4.11\times10^{-12}xT_e^3 + 7.26x10^{-13}xT_e^4 - 3.09\times10^{-14}xT_e^5$	78
I_3	$N_2 + e \rightarrow N_2^+ + 2e$	$1.01\times10^{-10}xT_e - 1.13\times10^{-10}xT_e^2 + 3.14\times10^{-11}xT_e^3 - 7.52x10^{-13}xT_e^4 - 5.14\times10^{-14}xT_e^5$	78
I_4	$H + e \rightarrow H^+ + 2e$	$6.50\times10^{-9}xT_e^{0.49}xe^{-12.89/Te}$	40[a]
I_5	$H_2 + e \rightarrow H^+ + H + 2e$	$3.00\times10^{-8}xT_e^{0.44}xe^{-37.72/Te}$	"
I_6	$H_2 + e \rightarrow H_2^+ + 2e$	$3.12\times10^{-8}xT_e^{0.17}xe^{-20.07/Te}$	"
I_7	$NH + e \rightarrow NH^+ + 2e$	$1.38\times10^{-10}xT_e - 1.85x10^{-10}xT_e^2 + 6.65x10^{-11}xT_e^3 - 4.36x10^{-12}xT_e^4 + 3.02x10^{-14}xT_e^5$	55
I_8	$NH + e \rightarrow N^+ + H + 2e$	$5.66\times10^{-11}xT_e - 6.91x10^{-11}xT_e^2 + 2.33x10^{-11}xT_e^3 - 1.96x10^{-12}xT_e^4 + 4.96x10^{-14}xT_e^5$	"
I_9	$NH_2 + e \rightarrow NH_2^+ + 2e$	$1.76x10^{-10}xT_e - 2.70x10^{-10}xT_e^2 + 1.17x10^{-10}xT_e^3 - 1.24x10^{-11}xT_e^4 + 4.23x10^{-13}xT_e^5$	"
I_{10}	$NH_2 + e \rightarrow NH^+ + H + 2e$	$1.08x10^{-10}xT_e - 1.28x10^{-10}xT_e^2 + 4.11x10^{-11}xT_e^3 - 2.91x10^{-12}xT_e^4 + 5.15x10^{-14}xT_e^5$	"
I_{11}	$NH_3 + e \rightarrow NH_3^+ + 2e$	$1.53x10^{-10}xT_e - 2.24x10^{-10}xT_e^2 + 9.37x10^{-11}xT_e^3 - 9.79x10^{-12}xT_e^4 + 3.33x10^{-13}xT_e^5$	"
I_{12}	$NH_3 + e \rightarrow NH_2^+ + H + 2e$	$1.57x10^{-10}xT_e - 2.02x10^{-10}xT_e^2 + 7.22x10^{-11}xT_e^3 - 6.69x10^{-12}xT_e^4 + 1.97x10^{-13}xT_e^5$	"
	Electron impact dissociation		
D_1	$H_2 + e \rightarrow 2H + e$	$1.75\times10^{-7}xT_e^{-1.24}xe^{-12.59/Te}$	40
D_2	$N_2 + e \rightarrow 2N + e$	$1.18\times10^{-8}x\,T_e^{0.5}xe^{-13.3/Te}$	49
D_3	$NH + e \rightarrow N + H + e$	$5.0x10^{-8}x\,T_e^{0.5}xe^{-8.6/Te}$	53
D_4	$NH_2 + e \rightarrow N + H_2 + e$	$5.0x10^{-8}xT_e^{0.5}xe^{-7.6/Te}$	52
D_5	$NH_2 + e \rightarrow NH + H + e$	$5.0x10^{-8}x\,T_e^{0.5}xe^{-7.6/Te}$	51,52
D_6	$NH_3 + e \rightarrow NH_2 + H + e$	$5.0x10^{-8}xT_e^{0.5}xe^{-4.4/Te}$	46
D_7	$NH_3 + e \rightarrow NH + H_2 + e$	$5.0x10^{-8}xT_e^{0.5}xe^{-5.5/Te}$	"
	Electron impact		
N_1	$H_2^+ + e \rightarrow H + H$	$7.51x10^{-9} - 1.12x10^{-9}xT_e + 1.03x10^{-10}xT_e^2 - 4.15x10^{-12}xT_e^3 + 5.86x10^{-14}xT_e^4$	40
N_2	$H_3^+ + e \rightarrow 3H$	$0.5xK^{(*)}$	"
N_3	$H_3^+ + e \rightarrow H_2 + H$	$0.5xK^{(*)}$	"
N_4	$N_2^+ + e \rightarrow N + N$	$2.8\times10^{-7}x(0.026/T_e)^{0.5}$	79
N_5	$NH^+ + e \rightarrow N + H$	$4.30x10^{-8}x(0.026/T_e)^{0.5}$	80
N_6	$NH_2^+ + e \rightarrow NH + H$	$1.02x10^{-7}x(0.026/T_e)^{0.40}$	81
N_7	$NH_2^+ + e \rightarrow N + 2H$	$1.98x10^{-7}x(0.026/T_e)^{0.40}$	"
N_8	$NH_3^+ + e \rightarrow NH + 2H$	$1.55x10^{-7}x(0.026/T_e)^{0.50}$	80
N_9	$NH_3^+ + e \rightarrow NH_2 + H$	$1.55x10^{-7}x(0.026/T_e)^{0.50}$	"
N_{10}	$NH_4^+ + e \rightarrow NH_3 + H$	$8.01x10^{-7}x(0.026/T_e)^{0.605}$	81
N_{11}	$NH_4^+ + e \rightarrow NH_2 + 2H$	$1.23x10^{-7}x(0.026/T_e)^{0.605}$	"
N_{12}	$N_2H^+ + e \rightarrow N_2 + H$	$7.1\times10^{-7}\,x(0.026/T_e)^{0.72}$	82
	Ion-molecule reaction		

T_1	$H^+ + NH_3 \rightarrow NH_3^+ + H$	5.20×10^{-9}	60
T_2	$H_2^+ + H \rightarrow H_2 + H^+$	6.4×10^{-10}	"
T_3	$H_2^+ + H_2 \rightarrow H_3^+ + H$	2.00×10^{-9}	"
T_4	$H_2^+ + NH_3 \rightarrow NH_3^+ + H_2$	5.70×10^{-9}	"
T_5	$H_2^+ + N_2 \rightarrow N_2H^+ + H$	2.00×10^{-9}	"
T_6	$H_3^+ + N \rightarrow NH^+ + H_2$	2.6×10^{-10}	"
T_7	$H_3^+ + N \rightarrow NH_2^+ + H$	3.9×10^{-10}	"
T_8	$H_3^+ + NH_3 \rightarrow NH_4^+ + H_2$	4.40×10^{-9}	"
T_9	$H_3^+ + N_2 \rightarrow N_2H^+ + H_2$	1.86×10^{-9}	"
T_{10}	$N^+ + H_2 \rightarrow NH^+ + H$	5.00×10^{-10}	"
T_{11}	$N^+ + NH_3 \rightarrow NH_2^+ + NH$	$0.20 \times 2.35 \times 10^{-9} = 4.7 \times 10^{-10}$	"
T_{12}	$N^+ + NH_3 \rightarrow NH_3^+ + N$	$0.71 \times 2.35 \times 10^{-9} = 1.67 \times 10^{-9}$	"
T_{13}	$N^+ + NH_3 \rightarrow N_2H^+ + H_2$	$0.09 \times 2.35 \times 10^{-9} = 2.12 \times 10^{-10}$	"
T_{14}	$NH^+ + H_2 \rightarrow H_3^+ + N$	$0.15 \times 1.23 \times 10^{-9} = 1.85 \times 10^{-10}$	"
T_{15}	$NH^+ + H_2 \rightarrow NH_2^+ + H$	$0.85 \times 1.23 \times 10^{-9} = 1.05 \times 10^{-9}$	"
T_{16}	$NH^+ + NH_3 \rightarrow NH_3^+ + NH$	$0.75 \times 2.40 \times 10^{-9} = 1.8 \times 10^{-9}$	"
T_{17}	$NH^+ + NH_3 \rightarrow NH_4^+ + N$	$0.25 \times 2.40 \times 10^{-9} = 6.0 \times 10^{-10}$	"
T_{18}	$NH^+ + N_2 \rightarrow N_2H^+ + N$	6.50×10^{-10}	"
T_{19}	$NH_2^+ + H_2 \rightarrow NH_3^+ + H$	1.95×10^{-10}	"
T_{20}	$NH_2^+ + NH_3 \rightarrow NH_3^+ + NH_2$	$0.5 \times 2.30 \times 10^{-9} = 1.15 \times 10^{-9}$	"
T_{21}	$NH_2^+ + NH_3 \rightarrow NH_4^+ + NH$	$0.5 \times 2.30 \times 10^{-9} = 1.15 \times 10^{-9}$	"
T_{22}	$NH_3^+ + NH_3 \rightarrow NH_4^+ + NH_2$	2.10×10^{-9}	"
T_{23}	$N_2^+ + H_2 \rightarrow N_2H^+ + H$	2.00×10^{-9}	"
T_{24}	$N_2^+ + NH_3 \rightarrow NH_3^+ + N_2$	1.95×10^{-9}	"
T_{25}	$N_2H^+ + NH_3 \rightarrow NH_4^+ + N_2$	2.30×10^{-9}	"

T_e is given in eV.

(*) $K = 8.39 \times 10^{-9} + 3.02 \times 10^{-9} \times T_e - 3.80 \times 10^{-10} \times T_e^2 + 1.31 \times 10^{-11} \times T_e^3 + 2.42 \times 10^{-13} \times T_e^4 - 2.30 \times 10^{-14} \times T_e^5 + 3.55 \times 10^{-16} \times T_e^6$

[a]The expressions for the rate coefficients of I_4, I_5, I_6, D_1, N_1, N_2 and N_3 are taken from ref. 40, where the original sources are indicated. The rate coefficient expressions for electron impact dissociation and ionization have been estimated in this work by using cross sections data and threshold energies taken from the indicated references. The rate coefficients for electron impact neutralization N_4-N_{12} and for ion-molecule reactions have been taken directly from the cited references.

Table 3. Wall neutralization and heterogeneous reactions

	Wall neutralization	**Rate coefficient**	**γ**
K_1	$H^+ + Wall \rightarrow H$	(eqn. 1)	1
K_2	$H_2^+ + Wall \rightarrow H_2$	(eqn. 1)	1
K_3	$H_3^+ + Wall \rightarrow H_2 + H$	(eqn. 1)	1
K_4	$N^+ + Wall \rightarrow N$	(eqn. 1)	1
K_5	$N_2^+ + Wall \rightarrow N_2$	(eqn. 1)	1
K_6	$NH^+ + Wall \rightarrow NH$	(eqn. 1)	1
K_7	$NH_2^+ + Wall \rightarrow NH_2$	(eqn. 1)	1
K_8	$NH_3^+ + Wall \rightarrow NH_3$	(eqn. 1)	1
K_9	$NH_4^+ + Wall \rightarrow NH_3 + H$	(eqn. 1)	1
K_{10}	$N_2H^+ + Wall \rightarrow N_2 + H$	(eqn. 1)	1
	Heterogeneous reactions		
W_1	$H + F_s \rightarrow H(s)$	(eqs. 2-3)	1
W_2	$H + H(s) \rightarrow H_2 + F_s$	(eqs. 5-6)	$1.5x10^{-3}$
W_3	$N + F_s \rightarrow N(s)$	(eqs. 2-3)	1
W_4	$N + N(s) \rightarrow N_2 + F_s$	(eqs. 5-6)	$6x10^{-3}$
W_5	$NH + F_s \rightarrow NH(s)$	(eqs. 2-3)	1
W_6	$NH_2 + F_s \rightarrow NH_2(s)$	(eqs. 2-3)	1
W_7	$N + H(s) \rightarrow NH(s)$	(eqs. 7-8)	$1x10^{-2}$
W_8	$H + N(s) \rightarrow NH(s)$	(eqs. 7-8)	$8x10^{-3}$
W_9	$H + NH(s) \rightarrow NH_2(s)$	(eqs. 7-8)	$8x10^{-3}$
W_{10}	$NH + H(s) \rightarrow NH_2(s)$	(eqs. 7-8)	$1x10^{-2}$
W_{11}	$NH(s) + H(s) \rightarrow NH_2(s) + F_s$	(eqn. 9)	-
W_{12}	$H + NH_2(s) \rightarrow NH_3 + F_s$	(eqs. 5-6)	$8x10^{-3}$
W_{13}	$NH_2 + H(s) \rightarrow NH_3 + F_s$	(eqs. 5-6)	$1x10^{-2}$
W_{14}	$H_2 + NH(s) \rightarrow NH_3 + F_s$	(eqs. 5-6)	$8x10^{-4}$
W_{15}	$NH_2(s) + H(s) \rightarrow NH_3 + 2F_s$	(eqn. 10)	-

F_s stands for a free surface site and X(s) refers to adsorbed species.

References

1 E. N. Eremin, A. N. Mal'tsev and V. M. Belova, *Russ. J. Phys. Chem.*, 1971, **45**, 635.
2 K.S. Yim and M. Venugopalan, *Plasma Chem. Plasma Process.*, 1983, **3**, 343.
3 K. Sugiyama, K. Akazawa, M. Oshima, H. Miura, T. Matsuda and O. Nomura, *Plasma Chem. Plasma Process.,* 1986, **6**, 179.
4 M. Touvelle, J. L. Muñoz-Licea and M. Venugopalan, *Plasma Chem. Plasma Process.*, 1987, **7**, 101.
5 J. Amorim, G. Bavarian and A. Ricard, *Plasma Chem. Plasma Process.*, 1995, **15**, 721.
6 H. Kiyooka and O. Matsumoto, *Plasma Chem. Plasma Process.,* 1996, **16**, 547.
7 A. Ricard, B.F. Gordiets, M.J. Pinheiro, C.M. Ferreira, G. Baravian, J. Amorim, S. Bockel and H. Michel, *Eur. Phys. J. AP*, 1998, **4**, 87.
8 B. Gordiets, C. M. Ferreira, M. J. Pinheiro and A. Ricard, *Plasma Sources Sci. Technol.,* 1998, **7**, 379.
9 P. Vankan, T. Rutten, S. Mazouffre, D. C. Schram and R. Engeln, *Appl. Phys. Lett.*, 2002, **81**, 418.
10 J. L. Jauberteau, I. Jauberteau and J. Aubreton*, J. Phys. D: Appl. Phys.*, 2002, **35**, 665.
11 J. H. van Helden, W. Wagemans, G. Yagci, R. A. B. Zijlmans, D. C. Schram, R. Engeln, G. Lombardi, G. D. Stancu and J. Röpcke, *J. Appl. Phys.*, 2007, **101**, 043305.
12 A. Garscadden and R. Nagpal, *Plasma Sources Sci. Technol.*, 1995, **4**, 268.
13 B. Gordiets, C. M. Ferreira, M. J. Pinheiro and A. Ricard, *Plasma Sources Sci. Technol.*, 1998, **7**, 363.
14 R. A. B. Zijlmans, PhD Thesis, *Molecule conversion in recombining plasmas,* Technical University Eindhoven, The Netherlands, 2008.
15 M. L. Steen, K. R. Kull and E. R. Fisher, *J. Appl. Phys.*, 2002, **92**, 55.
16 S. Xu, S. Y. Huang, I. Levchenko, H. P. Zhou, D. Y. Wei, S. Q. Xiao, L. X. Xu, W. S. Yan and K. Ostrikov, *Adv. Energy Mater.*, 2011, **1**, 373.
17 K. Ostrikov, U. Celvbar and A. B. Murphy, *J. Phys. D: Appl. Phys.*, 2011, **44**, 174001.
18 T. P. Ma, *IEEE Trans. Electron Devices*, 1998, **45**, 680.
19 A. G. Aberle, *Sol. Energy Mater. Sol. Cells*, 2001, **65**, 239.
20 D. L. Smith, A. S. Alimonda, C.C. Chen, S. E. Ready and B. Wacker*, J. Electrochem. Soc.*, 1990, **137**, 614.
21 D. T. Murley, R. A. G. Gibson, B. Dunnett, A. Goodyear and I. D. French, *J. Non-Cryst. Solids*, 1995, **187**, 324.
22 H. Umemoto, T. Morimoto, M. Yamawaki, Y. Masuda, A. Masuda and H. Matsumura, *Thin Solid Films*, 2003, **430**, 24.
23 P. J. van den Oever, J. H. van Helden, J. L. van Hemmen, R. Engeln, D. C. Schram, M. C. M. van de Sanden and W. M. M. Kessels, *J. Appl. Phys.*, 2006, **100**, 093303.
24 M. F. Romero, M. M. Sanz, I. Tanarro, A. Jiménez and E. Muñoz, *J. Phys. D: Appl. Phys.*, 2010, **43**, 495202.
25 G. Federici, C. H. Skinner, J. N. Brooks, J. P. Coad, C. Grisolia, A. A. Haasz, A. Hassanein, V. Philipps, C. S. Pitcher, J. Roth, W. R. Wampler and D. G. Whyte, *Nucl. Fusion*, 2001, **41**, 1967.
26 W. Jacob, C. Hopf, M. Meier and T. Schwarz-Selinger, in Nuclear Fusion Research: Understanding Plasma-Surface Interactions (Eds: R. E. H. Clark and D. Reiter), Springer Series in Chemical Physics Vol. 78, Springer Verlag, 2005.
27 J. Roth, E. Tsitrone, A. Loarte, Th. Loarer, G. Counsell, R. Neu, V. Philipps, S. Brezinsek, M. Lehnen, P. Coad, Ch. Grisolia, K. Schmid, K. Krieger, A. Kallenbach, B. Lipschultz, R.

Doerner, R. Causey, V. Alimov, W. Shu, O. Ogorodnikova, A. Kirschner, G. Federici and A. Kukushkin, *J. Nucl. Mater.*, 2009, **390–391**, 1.
28 F. L. Tabarés, D. Tafalla, I. Tanarro, V. J. Herrero, A. Islyaikin and C. Maffiotte, *Plasma Phys. Control. Fusion*, 2002, **44**, L37.
29 T. Schwarz-Selinger, C. Hopf, C. Sun and W. Jacob, *J. Nucl. Mat.*, 2007, **363**, 174.
30 I. Tanarro V. J. Herrero, A. M. Islyaikin, I. Méndez, F. L. Tabarés and D. Tafalla, *J. Phys. Chem. A,* 2007, **111**, 9003.
31 F. L. Tabarés, J. A. Ferreira, A. Ramos, G. van Rooij, J. Westerhout, R. Al, J. Rapp, A. Drenik and M. Mozetic, *Phys. Rev. Lett.*, 2010, **105**, 175006.
32 E. Herbst, *Chem. Soc. Rev.*, 2001, **30**, 168.
33 I. Lohmar, J. Krug and O. Biham, *Astron. Astrophys.*, 2009, **504**, L5.
34 P. Hall and T. J. Millar, *Astron. Astrophys.*, 2010, **517**, A1.
35 N. Watanabe and A. Kouchi, *Prog. Surf. Sci.*, 2008, **83**, 439.
36 D. J. Burke and W. A. Brown, *Phys. Chem. Chem. Phys.*, 2010, **12**, 5947.
37 S. Petrie and D. K. Bohme, *Mass Spectrom. Rev.*, 2007, **26**, 258.
38 E. Herbst and W. Klempere, *Astrophys. J.*, 1973, **185**, 505.
39 M. Womack, L.M. Ziurys and S. Wyckoff, *Astrophys. J.*, 1992, **393**, 188.
40 I. Méndez, F. J. Gordillo-Vázquez, V.J. Herrero and I. Tanarro*, J. Phys. Chem. A*, 2006, **110**, 6060.
41 M. Castillo, I. Méndez, A. M. Islyaikin, V. J. Herrero and I. Tanarro*, J. Phys. Chem. A*, 2005, **109**, 6255.
42 T. de los Arcos, C. Domingo, V. J. Herrero, M. M. Sanz, A. Schulz and I. Tanarro, *J. Phys. Chem. A,* 1998, **102**, 6282.
43 I. Tanarro and V. J. Herrero, *Plasma Sources Sci. Technol.*, 2009, **18**, 034007.
44 M. Castillo, V. J. Herrero and I. Tanarro, *Plasma Sources Sci. Tech.*, 2002, **11**, 368.
45 P. Pecher, Ph.D. Thesis, Quantitative Determination of the Particle Fluxes Emanating from Methane ECR Plasmas, Max-Planck-Institut Für Plasmaphysik, Germany, 1998.
46 H. Okabe, *Photochemistry of small molecules*, John Wiley & Sons Inc., 1978, pp. 270.
47 I. Tanarro, M.M. Sanz, D. Bermejo, C. Domingo and J. Santos, *J. Chem. Phys.*, 1994, **100**, 238.
48 D. R. Levine and R. B. Bernstein, *Molecular Reaction Dynamics*, Oxford University Press, 1987, pp. 59-61.
49 P. C. Cosby, *J. Chem. Phys.*, 1993, **98**, 9544.
50 K. Okada and S. Komatsu, *J. Appl. Phys.*, 1998, **84**, 6923.
51 H. Biehl, G. Schönnebeck, F. Stuhl and V. Staemmler, *J. Chem. Phys.*, 1994, **101**, 3819.
52 R. Vetter, L. Zülicke, A. Koch, E. F. van Dishoeck and S. D. Peyerimhoff, *J. Chem. Phys.*, 1996, **104**, 558.
53 L. C. Owono Owono, N. Jaidane, M. G. Kwato Njock and Z. Ben Lakhdar, *J. Chem. Phys.*, 2007, **126**, 244302.
54 J. Loureiro and C. M. Ferreira, *J. Phys. D: Appl. Phys.*, 1986, **19**, 17.
55 V. Tarnovsky, H. Deutsch and K. Becker, *Int. J. Mass Spectrom. Ion Processes*, 1997, **167/168**, 69-78.
56 R. Rejoub, B. G. Lindsay and R. F. Stebbings, *J. Chem. Phys.*, 2001, **115**, 5053.
57 P. Vankan, D.C. Schram and R. Engeln, *Chemical Physics Letters*, 2004, **400**, 196.
58 J. H. van Helden, R. Zijlmans, R. Engeln and D. C. Schram, *IEEE Transactions on Plasma Science*, 2005, **33**, 390.
59 J. P. van Helden, PhD Thesis, *The generation of molecules through plasma-surface*

interactions, Technical University Eindhoven, The Netherlands, 2006.
60 V. G. Anicich, *J. Phys. Chem. Ref. Data*, 1993, **22**, 1469. JPL publication 03-19 NASA, 2003.
61 M. Jiménez-Redondo, E. Carrasco, V. J. Herrero and I. Tanarro, *Phys. Chem. Chem. Phys.*, 2011, **13**, 9655.
62 V. Gencheva, R. Djulgerova, V. Mihailov, T. Dohnalik and Z. Lju Petrovic, *J. Phys. Conf. Ser.* 2007, **71**, 012009.
63 M. A. Lieberman and A. J. Lichtenberg, *Principles of plasma discharges and materials processing*, second edition, John Wiley & Sons, Inc., 2005.
64 P. Stoltze and J.K. Norskov, *J. Catal.*, 1988, **110**, 1.
65 R. D. Cortright and J. A. Dumesic, *Adv. Catal.*, 2001, **46**, 161.
66 P. J. Chantry, *J. Appl. Phys.*, 1987, **62**, 1141.
67 P. Kae-Nune, J. Perrin, J. Jolly and J. Guillo, *Surf. Sci. Lett.*, 1996, **360**, L495.
68 G. Ertl, S. B. Lee and M. Weiss, *Surf. Sci.*, 1982, **114**, 515.
69 F. Bozso, G. Ertl, M. Grunze and M. Weiss, *Appl. Surf. Sci.*, 1977, **1**, 103.
70 K. W. Kolasinski, Surface Science, John Wiley & Sons, 2002, pp. 86.
71 G. Ertl, *Catal. Rev. -Sci. Eng.*, 1980, **21**, 201.
72 J. V. Barth, *Surf. Sci. Rep.*, 2000, **40**, 70.
73 J. A. Dumesic and A. A. Treviño, *J. Catal.*, 1989, **116**, 119.
74 J. A. Dumesic, D.F. Rudd, L. M. Aparicio, J. E. Rekoske and A. A. Treviño, *The Microkinetics of Heterogeneous Catalysis*, American Chemical Society, Washington DC, 1993, pp. 29.
75 I. Tanarro and V. J. Herrero, *Plasma Sources Sci. Technol.*, 2011, **20**, 024006.
76 I. Méndez, I. Tanarro and V. J. Herrero, *Phys. Chem. Chem. Phys.*, 2010, **12**, 4239.
77 Y. Kim and J. P. Desclaux, *Phys. Rev. A*, 2002, **66**, 012708.
78 H. C. Straub, P. Renault, B. G. Lindsay, K. A. Smith, and R. F. Stebbings, *Phys. Rev. A*, 54, 2146 (1996).
79 I. A. Kossyi, A. Yu Kostinsky, A. A. Matyevev and V. P. Silakov, *Plasma Sources Sci. Technol.*, 1992, **1**, 207.
80 J. B. A. Mitchell, *Phys. Rep.*, 1990, **186**, 215.
81 L. Vikor, A. Al-Khalili, H. Danared, N. Djuric, G.H. Dunn, M. Larsson, A. Le Padellec, S. Rosén, and M. af Ugglas, *Astron. Astrophys.*, 1999, **344**, 1027.
82 T. Amano, *J. Chem. Phys.*, 1990, **92**, 6492.